Obstacle Avoidance via Hybrid Feedback

Berkane, Soulaimane; Bisoffi, Andrea; Dimarogonas, Dimos V.

Published in:
IEEE Transactions on Automatic Control

DOI:
10.1109/TAC.2021.3086329

Obstacle Avoidance via Hybrid Feedback

Soulaimane Berkane, *Member, IEEE*, Andrea Bisoffi, *Member, IEEE*, and Dimos V. Dimarogonas, *Senior Member, IEEE*

***Abstract*—In this article, we present a hybrid feedback approach to solve the navigation problem in the n-dimensional space containing an arbitrary number of ellipsoidal obstacles. The proposed algorithm guarantees both global asymptotic stabilization to a target position and avoidance of the obstacles. The controller, exploiting hysteresis regions, employs a Zeno-free switching between two modes of control: stabilization and avoidance. Simulation results illustrate the performance of the proposed approach for 2-D and 3-D scenarios.**

***Index Terms*—Asymptotic stability, autonomous vehicles, control design, collision avoidance, motion control, nonlinear control systems, Lyapunov methods.**

I. Introduction

For decades, the obstacle avoidance problem has been an active area of research in the robotics and control communities [1]. In a typical robot navigation scenario, the robot is required to reach a given goal (destination) while not colliding with a set of obstacle regions in the workspace. For this problem, the pioneering work [2] proposed to generate an artificial potential field that renders the goal attractive and the obstacles repulsive. Then, by navigating along the negative gradient of the artificial potential field, the robot will reach the desired target while avoiding collision with the obstacles. However, artificial potential field-based algorithms suffer from 1) the presence of local minima preventing the successful navigation to the target point and 2) arbitrarily large repulsive potential near the obstacles, which is in conflict with the inevitable actuator saturations. The navigation-function approach, initiated by Koditscheck and Rimon [3] for sphere worlds [3, p. 414], solves both problems. It allows obtaining artificial potential fields with the nice property that all critical points except one are saddles and the remaining critical point is the desired reference. Since then, the navigation-function-based approach has been extended in many different directions; e.g., for multiagent systems [4]–[6], for unknown sphere words [7], and for focally admissible obstacles [8]. The major drawback of navigation functions is that they are not correct by construction. In fact, navigation functions are theoretically guaranteed to exist, but their explicit computation is not straightforward since they require an unknown tuning of a given parameter to eliminate local minima. Recently, Loizou [9] introduced the navigation transform that diffeomorphically maps the workspace to a trivial domain called the *point world* consisting of a closed ball with a finite number of points removed. Once this transformation is found, the navigation problem is solved from almost all initial conditions without requiring any tuning. In addition, the trajectory duration is explicitly available, which provides a timed-abstraction solution to the motion-planning problem. Similarly, the recent work in [10] uses the so-called prescribed performance control to design a time-varying control law that drives the robot, in finite time, from all initial conditions to some neighborhood of the target while avoiding the obstacles. Another approach to the navigation problem is through barrier functions (see [11] and references therein), which are developed for nonlinear systems with state-space constraints and ensure safety. Model predictive control approaches have been also used for reactive robot navigation, e.g., [12], [13].

However, by using any of the approaches described earlier, it is not possible to ensure safety from all initial conditions in the obstacle-free state space. As pointed out in [3], the appearance of additional undesired equilibria is unavoidable when considering continuous time-invariant vector fields. Furthermore, this problem is more far-reaching since it is always possible to find arbitrarily small adversarial (noise) signals acting on the vector field, such that a set of initial conditions different from the target, possibly of measure zero, can be rendered stable [14, Th. 6.5]. To deal with such limitations, Sanfelice *et al.* [15] proposed a hybrid state feedback controller, using Lyapunov-based hysteresis switching, to achieve robust global asymptotic regulation in $\mathbb{R}^2$ to a target while avoiding a single obstacle. This approach has been exploited in [16] to steer a planar vehicle to the source of an unknown but measurable signal while avoiding an obstacle. In [17] and [18], a hybrid control law was proposed to globally asymptotically stabilize a class of linear systems while avoiding neighborhoods of unsafe isolated points in $\mathbb{R}^n$. Although such hybrid approaches are promising, they are still challenged by constructing the suitable hybrid feedback for higher dimensions and with more complex obstacles shapes.

In this article, we propose a hybrid control algorithm for the global asymptotic stabilization of a point mass moving in an arbitrary n-dimensional space while safely avoiding obstacles that have generic ellipsoidal shapes, based on the preliminary treatment of this problem for a single spherical obstacle in [19]. The ellipsoids provide a tighter bounding volume than spheres, and in our scheme, they can be arbitrarily flat and close to the target, which leads to a significant reduction in the level of conservatism compared, e.g., to [20, Th. 3] as we show in Section VI. Our proposed hybrid algorithm employs a hysteresis-based switching between the avoidance controller and the stabilizing controller to guarantee forward invariance of the obstacle-free region (corresponding to safety) and global asymptotic stability of the target position. We consider trajectories in an n-dimensional Euclidean space

Manuscript received February 15, 2021; accepted May 16, 2021. Date of publication June 3, 2021; date of current version December 29, 2021. This work was supported in part by the NSERC-DG RGPIN-2020-04759, in part by the European Research Council (ERC), in part by the EU H2020 Co4Robots, in part by the SSF COIN project, in part by the Swedish Research Council (VR), and in part by the Knut och Alice Wallenberg Foundation. Recommended by Associate Editor L. Wu. *(Corresponding author: Soulaimane Berkane.)*

Soulaimane Berkane is with the Department of Computer Science and Engineering, University of Quebec in Outaouais, Gatineau QC J8X 3X7, Canada (e-mail: berkane.soulaimane@gmail.com).

Andrea Bisoffi is with the ENTEG and the J.C. Willems Center for Systems and Control, University of Groningen, 9747 AG Groningen, The Netherlands (e-mail: a.bisoffi@rug.nl).

Dimos V. Dimarogonas is with the Division of Decision and Control Systems, KTH Royal Institute of Technology, 114 28 Stockholm, Sweden (e-mail: dimos@kth.se).

Color versions of one or more figures in this article are available at https://doi.org/10.1109/TAC.2021.3086329.

Digital Object Identifier 10.1109/TAC.2021.3086329

and we resort to tools from higher dimensional geometry to provide a construction of the flow and jump sets where the different modes of operation of the hybrid controller are activated. Furthermore, the hybrid control law guarantees a bounded control input, it matches the stabilizing controller in arbitrarily large subsets of the obstacle-free region by a suitable tuning of its parameters (hence qualifying as minimally invasive), it can be readily extended to a nonpoint mass vehicle and enjoys some level of inherent robustness to perturbations.

An extended version and all the proofs of the lemmas are in [21].

II. Preliminaries

$\mathbb{N}$, $\mathbb{R}$, and $\mathbb{R}_{\geq}$ denote, respectively, the set of nonnegative integers, reals, and nonnegative reals. $\mathbb{R}^n$ is the n-dimensional Euclidean space and $\mathbb{S}^n$ is the n-dimensional unit sphere embedded in $\mathbb{R}^{n+1}$. Given the column vectors $v_1 \in \mathbb{R}^{n_1}$ and $v_2 \in \mathbb{R}^{n_2}$, (v_1, v_2) denotes the stacked vector $\begin{bmatrix} v_1^\top & v_2^\top \end{bmatrix}^\top$. The Euclidean norm of $x \in \mathbb{R}^n$ is defined as $\|x\| := \sqrt{x^\top x}$. For an arbitrary matrix $A \in \mathbb{R}^{n\times n}$, $\lambda_i(A)$ denotes the ith eigenvalue of A. If A is a symmetric matrix, then $\lambda_{\min}(A)$ and $\lambda_{\max}(A)$ denote, respectively, the smallest and largest eigenvalue of A. The closure, interior, and boundary of a set $\mathcal{A} \subset \mathbb{R}^n$ are denoted as $\overline{\mathcal{A}}$, $\mathcal{A}^\circ$, and $\partial\mathcal{A}$, respectively. The relative complement of a set $\mathcal{B} \subset \mathbb{R}^n$ with respect to a set $\mathcal{A}$ is denoted by $\mathcal{A}\backslash\mathcal{B}$ and contains the elements of $\mathcal{A}$, which are not in $\mathcal{B}$. The tangent cone to a set $\mathcal{K} \subset \mathbb{R}^n$ at a point $x \in \mathbb{R}^n$, denoted $\mathbf{T}_{\mathcal{K}}(x)$, is defined as in [22, Def. 5.12 and Fig. 5.4]. For $z \in \mathbb{R}^n\backslash\{0\}$, we define the three projection maps

$$\pi^{\parallel}(z) := \tfrac{zz^\top}{\|z\|^2},\ \pi^{\perp}(z) := I_n - \tfrac{zz^\top}{\|z\|^2},\ \rho(z) := I_n - 2\tfrac{zz^\top}{\|z\|^2} \tag{1}$$

where I_n is the $n \times n$ identity matrix. The map $\pi^{\parallel}(\cdot)$ is the parallel projection map, $\pi^{\perp}(\cdot)$ is the orthogonal projection map [23], and $\rho(\cdot)$ is the reflector map (also called Householder transformation). For $v \neq 0$, $r \geq 0$, $2\theta \in [0, \pi]$ and E positive definite, we define the next geometric subsets of $\mathbb{R}^n$:

- line $\quad \mathcal{L}(c, v) := \{x \in \mathbb{R}^n : x = c + \lambda v, \lambda \in \mathbb{R}\}$ (2)
- hyperplane $\quad \mathcal{P}(c, v) := \{x \in \mathbb{R}^n : v^\top(x - c) = 0\}$ (3)
- sphere $\quad \mathcal{S}(c, r) := \{x \in \mathbb{R}^n : \|x - c\| = r\}$ (4)
- ellipsoid $\quad \mathcal{E}(c, E) := \{x \in \mathbb{R}^n : \|E(x - c)\|^2 = 1\}$ (5)
- cone $\quad \mathcal{C}(c,v,\theta,E) := \{x \in \mathbb{R}^n :$
$$\cos(\theta)\|Ev\|\|E(x - c)\| = v^\top E^2(x - c)\}. \tag{6}$$

In (3)–(6), we add subscripts $\leq$ or $\geq$ to refer to the set obtained by substituting the $=$ with $\leq$ or $\geq$. For example, $\mathcal{P}_{\leq}(c, v)$ and $\mathcal{P}_{\geq}(c, v)$ are the two closed sets into which the hyperplane $\mathcal{P}(c, v)$ divides $\mathbb{R}^n$.

Definition 1: Two ellipsoids $\mathcal{E}_{\leq}(c_1, E_1)$ and $\mathcal{E}_{\leq}(c_2, E_2)$ are weakly disjoint if $\mathcal{E}_{\leq}(c_1, E_1) \cap \mathcal{E}_{\leq}(c_2, E_2) = \emptyset$, and are strongly disjoint if $(\lambda_{\min}(E_1))^{-1} + (\lambda_{\min}(E_2))^{-1} < \|c_1 - c_2\|$.

Strong disjointness means that the two smallest spherical balls containing the ellipsoids are disjoint and is more conservative than weak disjointness. We use hybrid dynamical systems [22], i.e.,

$$\begin{cases} \dot{X} \in \mathbf{F}(X), & X \in \mathcal{F} \\ X^+ \in \mathbf{J}(X), & X \in \mathcal{J} \end{cases} \tag{7}$$

where $X \in \mathbb{R}^n$ is the state, the (set-valued) *flow map* $\mathbf{F} : \mathbb{R}^n \rightrightarrows \mathbb{R}^n$ and *jump map* $\mathbf{J} : \mathbb{R}^n \rightrightarrows \mathbb{R}^n$ govern continuous and discrete evolution, which can occur, respectively, in the *flow set* $\mathcal{F} \subset \mathbb{R}^n$ and the *jump set* $\mathcal{J} \subset \mathbb{R}^n$. The notions of solution ϕ to a hybrid system, its hybrid time domain $\operatorname{dom}\phi$, maximal and complete solution are, respectively, as in [22, Def. 2.6, Def. 2.3, Def. 2.7, p. 30].

III. Problem Formulation

We consider a point mass vehicle moving in the n-dimensional Euclidean space containing $I \in \mathbb{N}$ obstacles denoted by $\mathcal{O}_1, \ldots, \mathcal{O}_I$. For each $i \in \{1, \ldots, I\} =: \mathbb{I}$, the obstacle $\mathcal{O}_i$ has an ellipsoidal shape such that $\mathcal{O}_i := \mathcal{E}_{\leq}(c_i, E_i)$, for some center $c_i \in \mathbb{R}^n$ and some positive definite matrix $E_i \in \mathbb{R}^{n\times n}$ defining the shape of the obstacle. The free workspace is then defined by the closed set

$$\mathcal{W} := \bigcap_{i\in\mathbb{I}} \mathcal{E}_{\geq}(c_i, E_i). \tag{8}$$

The vehicle is moving according to the dynamics

$$\dot{x} = u \tag{9}$$

where $x \in \mathbb{R}^n$ is the state and $u \in \mathbb{R}^n$ is the control input. The vehicle is required to stabilize its position to a target position while avoiding the obstacles. Without loss of generality we consider the target position to be the origin $x = 0$.

Assumption 1: $n \geq 2$.

We consider $n \geq 2$ since for $n = 1$ (i.e., the state space is a line), global asymptotic stabilization with obstacle avoidance is infeasible.

Assumption 2: For all $i \in \mathbb{I}$, $\|E_i c_i\| > 1$.

Assumption 2 requires that the target position $x = 0$ is not inside any of the obstacle regions $\mathcal{O}_i$, otherwise the considered navigation problem would be infeasible.

Assumption 3: $\{\mathcal{O}_i\}_{i\in\mathbb{I}}$ are weakly pairwise disjoint.

In Assumption 3, we impose that there is no intersection region between any two obstacles. Our *objectives* in designing a control strategy are

1) the obstacle-free region $\mathcal{W}$ in (8) is forward invariant (that is, the free workspace $\mathcal{W}$ is safe);
2) the target $x = 0$ is globally asymptotically stable.

IV. Hybrid Control for Obstacle Avoidance

A. Control Input

In this section, we propose the feedback law for the control input u in (9). We define a discrete variable

$$m \in \{-1, 0, 1\} =: \mathbb{M}.$$

The value $m = 0$ corresponds to the activation of the stabilizing controller and the values $m = -1$, $m = 1$ correspond to the activation of one of the two configurations of the avoidance controller. The proposed control input u depends on the state $x \in \mathbb{R}^n$, the obstacle $i \in \mathbb{I}$ and the control mode $m \in \mathbb{M}$ as

$$u = \kappa(x, i, m) := \begin{cases} -k_0 x, & m = 0 \\ -k_m E_i^{-1}\pi^{\perp}(E_i(x - c_i))E_i(x - p_m^i), & m \in \{-1, 1\} \end{cases} \tag{10}$$

where k_{-1}, k_0, $k_1 > 0$ are the control gains for each control mode $m \in \mathbb{M}$ and the points $p_m^i \in \mathbb{R}^n$, $m \in \{-1, 1\}$ and $i \in \mathbb{I}$, are design parameters defined later. In the stabilization mode ($m = 0$), the control input in (10) steers x toward the origin through state feedback. In the avoidance mode depicted in Fig. 1, the control input minimizes the distance to the *auxiliary* attractive point p_m^i *while* maintaining a constant distance to the obstacle $\mathcal{O}_i$. Indeed, the time derivative of $\|E_i(x - c_i)\|^2$ along solutions of $\dot{x} = \kappa(x, i, m)$ for $m \in \{-1, 1\}$ and $i \in \mathbb{I}$, is zero. Then, if we activate the avoidance mode sufficiently away from the obstacle, the avoidance feedback $u = \kappa(x, i, m)$ guarantees that the vehicle does not hit the obstacle. Whereas the logic variable i corresponds to obstacle $\mathcal{O}_i$, the logic variable m is selected according

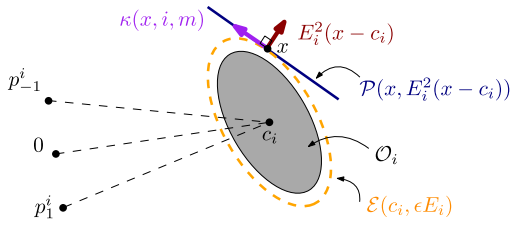

Fig. 1. Illustration of the projection-based avoidance controller. The vehicle is attracted to an auxiliary point p_m^i while sliding on a neighboring ellipsoid.

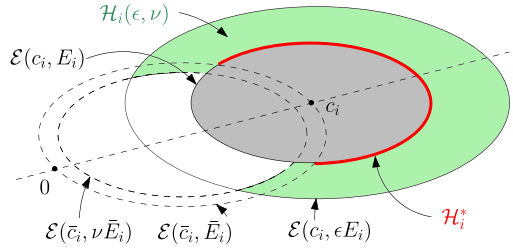

Fig. 2. Helmet $\mathcal{H}_i^*$ in (13) (red) corresponds to all boundary points where the stabilization vector field is pointing inside the obstacle (grey). The safety helmet $\mathcal{H}_i(\epsilon,\nu)$ in (14) (green) corresponds to a dilated version of $\mathcal{H}_i^*$.

to a hybrid mechanism that exploits a suitable construction of flow and jump sets, detailed in Section IV-B.

In order to clear the obstacle while approaching the desired target position at the origin, we select the points p_1^i and p_{-1}^i in the region between the obstacle and the origin, see Fig. 1. More precisely, for $\theta_i > 0$ (which will be further bounded in Lemma 3), the points p_1^i and p_{-1}^i are selected as

$$p_1^i \in \mathcal{C}(c_i,-c_i,\theta_i,E_i)\backslash\{c_i\} \tag{11a}$$

$$p_{-1}^i := -E_i^{-1}\rho(E_ic_i)E_ip_1^i. \tag{11b}$$

By (11), p_{-1}^i opposes p_1^i diametrically with respect to the cone axis (for $E_i = I_n$, p_{-1}^i is obtained by an orthogonal reflection) and also belongs to $\mathcal{C}(c_i,-c_i,\theta_i,E_i)\backslash\{c_i\}$ as shown in the next lemma.

Lemma 1: $p_{-1}^i \in \mathcal{C}(c_i,-c_i,\theta_i,E_i)\backslash\{c_i\}$.

Note that the results of this article hold for any selection of the point p_1^i as long as it lies on the surface of the cone as in (11a). An explicit guided choice for the points p_1^i is given in Section VI for the 2-D and 3-D cases. The motivation for the choice of the avoidance controller mode in (10) is that the avoidance task is analogous (up to a linear transformation) to a stabilization problem on the unit sphere $\mathbb{S}^{n-1}$. Therefore, as pointed out for instance in [24], global asymptotic stabilization cannot be accomplished by only one continuous time-invariant controller, but it can be by a hybrid feedback with at least two configurations. For this reason, we consider two avoidance modes with $m=-1$ and $m=1$ and, hence, the points p_1^i and p_{-1}^i must be distinct. Further motivation for this construction is detailed in Section IV-B.

B. Geometric Construction of the Flow and Jump Sets

In this section, we construct explicitly the flow and jump sets where the stabilization and avoidance controllers are activated.

1) Safety Helmets: Our proposed construction of flow and jump sets is based on regions that have the shape of a *helmet*, whose construction is now motivated. In the stabilization mode $m=0$, the closed-loop system should *not* flow when: 1) x is close enough to any of the obstacle regions $\mathcal{E}_{\leq}(c_i,E_i)$ and 2) the vector field $-k_0x$ points inside $\mathcal{E}_{\leq}(c_i,E_i)$. Otherwise, the vehicle ends up hitting the obstacle i. Indeed, by computing the time derivative of $\|E_i(x-c_i)\|^2$ along solutions of the vector field $-k_0x$, we obtain

$$\tfrac{1}{2}\tfrac{d}{dt}\|E_i(x-c_i)\|^2 = k_0\|E_i\bar{c}_i\|^2\left(1-\|\bar{E}_i(x-\bar{c}_i)\|^2\right) \tag{12}$$

where $\bar{c}_i := c_i/2$ and $\bar{E}_i := 2E_i/(\|E_ic_i\|)$. Equation (12) implies that the distance function $\|E_i(x-c_i)\|^2$ decreases for all x in the closed set $\mathcal{E}_{\geq}(\bar{c}_i,\bar{E}_i)$. Consider now Fig. 2 for a sketch of the next sets. For obstacle i, define the *helmet*-shaped set

$$\mathcal{H}_i^* := \mathcal{E}(c_i,E_i)\cap\mathcal{E}_{\geq}(\bar{c}_i,\bar{E}_i). \tag{13}$$

$\mathcal{H}_i^*$ is the set of all points that lie on the boundary of the obstacle $\mathcal{O}_i$ and are associated with a vector field pointing toward the obstacle. Then, for obstacle i, we define the *safety helmet* as

$$\mathcal{H}_i(\epsilon,\nu) := \mathcal{E}_{\leq}(c_i,\epsilon E_i)\cap\mathcal{E}_{\geq}(c_i,E_i)\cap\mathcal{E}_{\geq}(\bar{c}_i,\nu\bar{E}_i) \tag{14}$$

for some parameters $\epsilon,\nu>0$. ϵ and ν determine the thickness of the safety helmet by tuning the dilation/shrinking of the ellipsoids $\mathcal{E}(c_i,E_i)$ and $\mathcal{E}(\bar{c}_i,\bar{E}_i)$, thereby generating a dilated version of $\mathcal{H}_i^*$. The safety helmet $\mathcal{H}_i(\epsilon,\nu)$ constitutes the main ingredient of our following constructions.

2) Stabilization Mode $m=0$: Consider Fig. 3 from now on for a visualization of the sets we are introducing in our construction. In stabilization mode ($m=0$), we create around each obstacle $\mathcal{O}_i$ a safety helmet $\mathcal{H}_i(\epsilon_i,\nu_i)$ that adds a safety layer to the given obstacle. The controller mode must be switched to the avoidance mode whenever the vehicle reaches this safety helmet. Specifically, we define for each $i\in\mathbb{I}$, a jump set

$$\mathcal{J}_0^i := \mathcal{H}_i(\epsilon_i,\nu_i)\cap\mathcal{W} \tag{15}$$

where $\epsilon_i\in(0,1)$ dilates $\mathcal{E}_{\leq}(c_i,E_i)$ to $\mathcal{E}_{\leq}(c_i,\epsilon_iE_i)$, $\nu_i\in(1,\infty)$ shrinks $\mathcal{E}_{\geq}(\bar{c}_i,\bar{E}_i)$ to $\mathcal{E}_{\geq}(\bar{c}_i,\nu_i\bar{E}_i)$, and $\mathcal{W}$ is the free workspace defined in (8). We emphasize that we consider the intersection with $\mathcal{W}$ in (15) for convenience, but later we tune the parameters such that $\mathcal{H}_i(\epsilon_i,\nu_i)\subset\mathcal{W}$, which implies $\mathcal{J}_0^i$ will equal to $\mathcal{H}_i(\epsilon_i,\nu_i)$. The selection of $\mathcal{J}_0^i$ in (15) leads naturally to the next set (corresponding to the closed complement of $\mathcal{J}_0^i$ in the free workspace)

$$\mathcal{F}_0^i := \left(\mathcal{E}_{\geq}(c_i,\epsilon_iE_i)\cup\mathcal{E}_{\leq}(\bar{c}_i,\nu_i\bar{E}_i)\right)\cap\mathcal{W}, \tag{16}$$

which we use for the flow set of the stabilization mode. Finally, from (15) and (16), we take all the obstacles into account and define the flow and jump sets for the stabilization mode as

$$\mathcal{F}_0 := \left(\bigcap_{i\in\mathbb{I}}\mathcal{F}_0^i\right)\times\mathbb{I}, \qquad \mathcal{J}_0 := \left(\bigcup_{i\in\mathbb{I}}\mathcal{J}_0^i\right)\times\mathbb{I}. \tag{17}$$

Indeed, the stabilization mode will be selected when the state x belongs to the intersection of the sets $\mathcal{F}_0^i$, and a jump to the avoidance mode will occur when the state x belongs to the union of the sets $\mathcal{J}_0^i$. In other words, if during the stabilization mode the vehicle reaches any one of the safety helmets, then the controller jumps to one of the avoidance modes with m equal to -1 or 1.

3) Avoidance Mode $m\in\{-1,1\}$: We consider now the construction of flow and jump sets for the avoidance modes $m\in\{-1,1\}$ and the specific obstacle $i\in\mathbb{I}$ with the aid of Fig. 3. To highlight their motivation, we first define such flow sets and state later in (20) the corresponding jump sets. For each $i\in\mathbb{I}$ and $m\in\{-1,1\}$, the avoidance flow set is

$$\mathcal{F}_m^i := \mathcal{H}_i(\delta_i,\mu_i)\cap\mathcal{C}_{\geq}(c_i,c_i-p_m^i,\psi_i,E_i)\cap\mathcal{W} \tag{18}$$

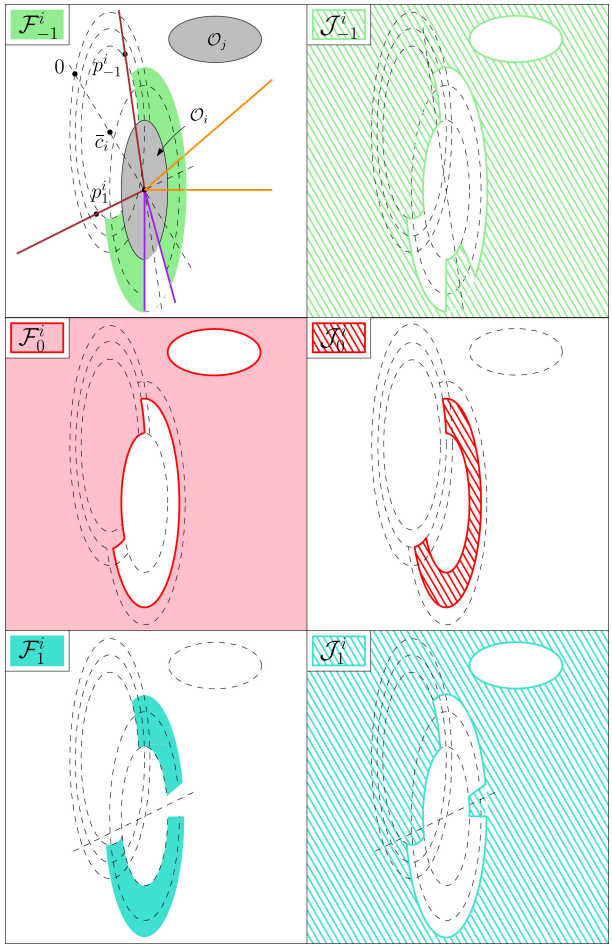

Fig. 3. 2-D illustration of flow and jump sets considered in Sections IV and V corresponding to obstacle $\mathcal{O}_i$ (in the presence of a second obstacle $\mathcal{O}_j$). The stabilization-mode jump set $\mathcal{J}^i_0$ (hatched red) is constructed by using the helmet $\mathcal{H}_i(\epsilon_i, \nu_i)$, whereas the corresponding flow set $\mathcal{F}^i_0$ is the complement of $\mathcal{J}^i_0$ in the free workspace. For the avoidance mode we select p^i_1 and p^i_{-1} to lie on the cone $\mathcal{C}(c_i, -c_i, \theta_i, E_i)$ (solid brown line). The avoidance flow set $\mathcal{F}^i_m$, with $m \in \{-1, 1\}$, corresponds to the helmet $\mathcal{H}_i(\delta_i, \mu_i)$ deprived of the interior of the cone region defined by $\mathcal{C}(c_i, c_i - p^i_m, \psi_i, E_i)$ (solid purple line for $m = -1$ and solid orange line for $m = 1$). The corresponding jump set $\mathcal{J}^i_m$ is the complement of $\mathcal{F}^i_m$ in the free workspace.

with $\delta_i \in (0, \epsilon_i)$ dilating $\mathcal{E}_{\leq}(c_i, \epsilon_i E_i)$ to $\mathcal{E}_{\leq}(c_i, \delta_i E_i)$, $\mu_i \in (\nu_i, \infty)$ shrinking $\mathcal{E}_{\geq}(\bar{c}_i, \nu_i \bar{E}_i)$ to $\mathcal{E}_{\geq}(\bar{c}_i, \mu_i \bar{E}_i)$, and $\psi_i \in (0, \pi/2]$. In the two configurations $m \in \{-1, 1\}$ of the avoidance of obstacle $i \in \mathbb{I}$, we want the vehicle to slide on the safety helmet $\mathcal{H}_i(\delta_i, \mu_i)$ while maintaining a constant distance to the obstacle. By selecting $\delta_i \in (0, \epsilon_i)$ and $\mu_i \in (\nu_i, \infty)$, one obtains a dilated version of $\mathcal{H}_i(\epsilon_i, \nu_i)$ used in $\mathcal{J}^i_0$ and, thus, creates a hysteresis region useful to prevent infinitely many consecutive jumps (Zeno behavior). However, the avoidance vector field $\kappa(x, i, m)$ in (10) has some undesirable equilibria, which we need to rule out from the flow sets $\mathcal{F}^i_1$ and $\mathcal{F}^i_{-1}$ and we characterize in the next lemma.

Lemma 2: Let $c \in \mathbb{R}^n$, $p \in \mathbb{R}^n \backslash \{c\}$ and $E \in \mathbb{R}^{n \times n}$ positive definite. For each $x \in \mathbb{R}^n \backslash \{c\}$, $\pi^{\perp}(E(x-c))E(x-p) = 0$ if and only if $x \in \mathcal{L}(c, p-c)$.

For each $m \in \{-1, 1\}$, $i \in \mathbb{I}$, we want solutions to eventually leave the set $\mathcal{F}^i_m$ of the avoidance mode, so it is necessary to select point p^i_m and flow set $\mathcal{F}^i_m$ such that $\mathcal{L}(c_i, p^i_m - c_i) \cap \mathcal{F}^i_m = \emptyset$ based on Lemma 2, otherwise solutions could stay in avoidance mode indefinitely. This motivates the intersection with the cone in (18), and the next lemma.

TABLE I
SELECTION OF THE DESIGN PARAMETERS OF (22), WITH $i \in \mathbb{I}$

Parameter	Selection	Parameter	Selection
δ_i	$(\underline{\delta}_i, 1)$	ϵ_i	$(\delta_i, 1)$
μ_i	$(1, \bar{\mu}_i(\delta_i))$	ν_i	$(1, \mu_i)$
θ_i	$(0, \bar{\theta}_i(\delta_i, \mu_i))$	$\bar{\psi}_i$	$(0, \theta_i)$
$k_0,\ k_1,\ k_{-1}$	$(0, +\infty)$	ψ_i	$(0, \bar{\psi}_i)$
		$p^i_1,\ p^i_{-1}$	as in (11)

Lemma 3: For each $i \in \mathbb{I}$, define the quantities

$$\underline{\delta}_i := \|E_i c_i\|^{-\frac{1}{2}} \tag{19a}$$

$$\bar{\mu}_i(\delta_i) := \left(1 - 4\underline{\delta}_i^2 (1 - \underline{\delta}_i^2/\delta_i^2)\right)^{-\frac{1}{2}} \tag{19b}$$

$$\bar{\theta}_i(\delta_i, \mu_i) := \arccos\left(\frac{\underline{\delta}_i^2}{\delta_i^2} + \frac{1}{4\underline{\delta}_i^2}\left(1 - \frac{1}{\mu_i^2}\right)\right) \tag{19c}$$

and select the parameters $\delta_i, \mu_i, \theta_i, \psi_i$ as in Table I so that $\bar{\mu}_i(\delta_i)$ and $\bar{\theta}_i(\delta_i, \mu_i)$ are well defined. Then, for each $m \in \{-1, 1\}$, $\mathcal{L}(c_i, p^i_m - c_i) \cap \mathcal{F}^i_m = \emptyset$.

From the flow set in (18), we suitably define the jump set for the avoidance mode, of an obstacle $i \in \mathbb{I}$ with configuration $m \in \{-1, 1\}$, to be the closed complement of $\mathcal{F}^i_m$ in the free workspace. For $i \in \mathbb{I}$ and $m \in \{-1, 1\}$

$$\mathcal{J}^i_m := \left(\mathcal{E}_{\geq}(c_i, \delta_i E_i) \cup \mathcal{E}_{\leq}(\bar{c}_i, \mu_i \bar{E}_i) \cup \mathcal{C}_{\leq}(c_i, c_i - p^i_m, \psi_i, E_i)\right) \cap \mathcal{W}. \tag{20}$$

Finally, the avoidance mode has overall flow and jump sets

$$\mathcal{F}_1 := \bigcup_{i \in \mathbb{I}} \left(\mathcal{F}^i_1 \times \{i\}\right), \qquad \mathcal{J}_1 := \bigcup_{i \in \mathbb{I}} \left(\mathcal{J}^i_1 \times \{i\}\right) \tag{21a}$$

$$\mathcal{F}_{-1} := \bigcup_{i \in \mathbb{I}} \left(\mathcal{F}^i_{-1} \times \{i\}\right), \qquad \mathcal{J}_{-1} := \bigcup_{i \in \mathbb{I}} \left(\mathcal{J}^i_{-1} \times \{i\}\right) \tag{21b}$$

where $\mathcal{F}^i_m$ and $\mathcal{J}^i_m$ ($m \in \{-1, 1\}$) are defined in (18) and (20). Indeed, *each* obstacle i gives rise, for the avoidance mode, to a specific flow (jump) set with two configurations $\mathcal{F}^i_1$ and $\mathcal{F}^i_{-1}$ ($\mathcal{J}^i_1$ and $\mathcal{J}^i_{-1}$), as we motivated in this section.

C. Hybrid Mode Selection

In this section, we define the hybrid switching strategy that permits a Zeno-free transition between the different control modes. The hybrid selection of the logical variables $i \in \mathbb{I}$ and $m \in \mathbb{M}$ is implemented in the hybrid system

$$\begin{cases} \dot{x} = \kappa(x, i, m), \\ \dot{\hat{i}} = 0, \\ \dot{m} = 0, \end{cases} \qquad (x, i, m) \in \mathcal{F} \tag{22a}$$

$$\begin{cases} x^+ = x, \\ \begin{bmatrix} i^+ \\ m^+ \end{bmatrix} \in \mathbf{L}(x, i, m), \end{cases} \qquad (x, i, m) \in \mathcal{J} \tag{22b}$$

where $\kappa(x, i, m)$ is the control input defined in (10) and the flow and jump sets are given by

$$\mathcal{F} := \bigcup_{m \in \mathbb{M}} \left(\mathcal{F}_m \times \{m\}\right), \qquad \mathcal{J} := \bigcup_{m \in \mathbb{M}} \left(\mathcal{J}_m \times \{m\}\right) \tag{22c}$$

with $\mathcal{F}_m$ and $\mathcal{J}_m$ being defined in (17) for $m = 0$ and in (21a)–(21b) for $m \in \{-1, 1\}$. We define now the (set-valued) jump map $\mathbf{L}$ in (22b). To this end, for $i \in \mathbb{I}$ and $m \in \{-1, 1\}$, define the sets $\mathcal{C}_m^i$ as

$$\mathcal{C}_m^i := \mathcal{C}_{\geq}(c_i, c_i - p_m^i, \bar{\psi}_i, E_i), \tag{22d}$$

which corresponds to the region outside the cone with vertex at c_i, axis $c_i - p_m^i$ and aperture $2\bar{\psi}_i$, where $\bar{\psi}_i$ is a design parameter selected later. The jump map $\mathbf{L}$ for $m \in \{-1, 1\}$ is then defined as

$$\mathbf{L}(x, i, -1) := \mathbf{L}(x, i, 1) := \left\{ \begin{bmatrix} i \\ 0 \end{bmatrix} \right\}, \tag{22e}$$

i.e., when jumping to stabilization mode, the obstacle index i is not used in the control law κ in (10) and consequently is not updated. The jump map $\mathbf{L}$ for $m = 0$ is

$$\mathbf{L}(x, i, 0) := \left\{ \begin{bmatrix} i' \\ m' \end{bmatrix} : x \in \mathcal{J}_0^{i'}, m' \in \mathbf{M}(x, i') \right\} \tag{22f}$$

where $\mathbf{M}$ is defined, based on (22d), as

$$\mathbf{M}(x, i) := \begin{cases} \{-1\}, & x \in \mathcal{C}_{-1}^i \backslash \mathcal{C}_1^i \\ \{1\}, & x \in \mathcal{C}_1^i \backslash \mathcal{C}_{-1}^i \\ \{-1, 1\}, & x \in \mathcal{C}_{-1}^i \cap \mathcal{C}_1^i. \end{cases} \tag{22g}$$

$\mathbf{L}(\cdot, \cdot, 0)$ captures that when jumping from the stabilization mode $m = 0$, the suitable avoidance mode of obstacle $i' \in \mathbb{I}$ with configuration $m' \in \{-1, 1\}$ is selected based on the position x of the vehicle (m', in particular, is selected based on whether x is within the cone region $\mathcal{C}_{-1}^{i'}$ or $\mathcal{C}_1^{i'}$). A necessary condition to implement our hybrid controller is that the jump map is nonempty, for which we have the next lemma.

Lemma 4: Select the parameters $\bar{\psi}_i$ and ψ_i as in Table I. Then, the set $\mathbf{L}(x, i, m)$ is nonempty for all $(x, i, m) \in \mathcal{J}$.

For compact notation, we write flow and jump maps as

$$(x, i, m) \mapsto \mathbf{F}(x, i, m) := (\kappa(x, i, m), 0, 0) \tag{22h}$$

$$(x, i, m) \rightrightarrows \mathbf{J}(x, i, m) := (x, \mathbf{L}(x, i, m)) \tag{22i}$$

and the overall state of the hybrid system as

$$\xi := (x, i, m) \in \mathbb{R}^n \times \mathbb{I} \times \mathbb{M}. \tag{22j}$$

This completes the description of the hybrid controller in (22). The selections we made in this section for the parameters of (22) are summarized in Table I.

V. Main Results

In this section, we show that the hybrid controller achieves forward invariance and global asymptotic stability, as well as some complementary properties. The mild regularity conditions satisfied by the hybrid system (22), as in the next lemma, allow us to invoke useful results on hybrid systems for proving our results.

Lemma 5: The hybrid system with data $(\mathcal{F}, \mathbf{F}, \mathcal{J}, \mathbf{J})$ satisfies the hybrid basic conditions in [22, Assumption 6.5].

A. Forward Invariance

Since the state x must evolve always within the free workspace $\mathcal{W}$ in (8) regardless of the logic variables i and m, we seek forward invariance of the set $\mathcal{K}$ defined as

$$\mathcal{K} := \bigcap_{i \in \mathbb{I}} \mathcal{E}_{\geq}(c_i, E_i) \times \mathbb{I} \times \mathbb{M} = \mathcal{W} \times \mathbb{I} \times \mathbb{M}. \tag{23}$$

The next lemma shows that the union of flow and jump sets covers exactly the obstacle-free state space $\mathcal{K}$ and that solutions cannot leave $\mathcal{K}$ through jumps.

Lemma 6: $\mathcal{F} \cup \mathcal{J} = \mathcal{K}$ and $\mathbf{J}(\mathcal{J}) \subset \mathcal{K}$.

Forward invariance of $\mathcal{K}$ holds by the next theorem, proven in the Appendix.

Theorem 1: Under Assumptions 1–3, consider the hybrid system (22) with parameters selected as in Table I. Assume also that the controller parameters δ_i are tuned so that the ellipsoids $\{\mathcal{E}_{\leq}(c_i, \delta_i E_i)\}_{i \in \mathbb{I}}$ are weakly pairwise disjoint. Then, the obstacle-free set $\mathcal{K}$ in (23) is forward invariant.

The existence of tuning parameters $\delta_1, \ldots, \delta_I$ satisfying the weak pairwise disjointness of the sets $\{\mathcal{E}_{\leq}(c_i, \delta_i E_i)\}_{i \in \mathbb{I}}$ is guaranteed by Assumption 3, which implies that weak pairwise disjointness holds when $\delta_i = 1$ for all $i \in \mathbb{I}$. Hence, by a continuity argument, we can always tune each δ_i sufficiently close to 1 in order to guarantee the weak pairwise disjointness of the dilated obstacles $\{\mathcal{E}_{\leq}(c_i, \delta_i E_i)\}_{i \in \mathbb{I}}$. Algebraic tests of weak pairwise disjointness (in [25, Th. 6] for $n = 2$ and in [26, Th. 8] for $n = 3$) can be used for this tuning.

B. Global Asymptotic Stability

We show that from all initial conditions in the free workspace, all solutions converge asymptotically to the origin. To this end, we define the notion of *sufficient disjointness* of a set of ellipsoids, which is slightly stronger than weak disjointness but less conservative than strong disjointness, and guarantees that each obstacle is avoided at most one time. The motivation behind the assumption of sufficient disjointness is that the arbitrarily large and flat ellipsoids considered here may lead to long avoidance-mode detours that take the vehicle far away from the origin and can prevent from converging to it for specific obstacles configurations. Similarly, this occurs in the Bug *0* planning algorithm [27], where convergence to the origin is not *always* guaranteed since the algorithm is designed to "walk toward the target whenever you can" [27], and our hybrid feedback shares a similar philosophy, see (12) and Section IV.B. To proceed, the next lemma characterizes the intersection of two ellipsoids of interest.

Lemma 7: Consider an arbitrary $i \in \mathbb{I}$. For $\underline{\delta}_i$, $\delta \mapsto \bar{\mu}_i(\delta)$ and $(\delta, \mu) \mapsto \bar{\theta}_i(\delta, \mu)$ defined in (19), let $\delta \in [\underline{\delta}_i, 1]$, $\mu \in [1, \bar{\mu}_i(\delta)]$ and $\vartheta_i(\delta, \mu)$ be such that

$$\cos(\vartheta_i(\delta, \mu)) := \frac{1 - \cos(\bar{\theta}_i(\delta, \mu))\underline{\delta}_i^2}{\sqrt{(1 + \mu^{-2})/2 - \delta^{-2}\underline{\delta}_i^4}}. \tag{24}$$

The expression in (24) is well defined and positive, and

$$\mathcal{E}(c_i, \delta E_i) \cap \mathcal{E}(\bar{c}_i, \mu \bar{E}_i) \subset \mathcal{C}(0, c_i, \vartheta_i(\delta, \mu), E_i). \tag{25}$$

Let us consider for each obstacle $i \in \mathbb{I}$ the sphere $\mathcal{S}(0, \bar{r}_i)$ with center at the origin and radius $\bar{r}_i$ defined by $\bar{r}_i^2 := \min\{\|x\|^2 : x \in \mathcal{H}_i^*\}$ where $\mathcal{H}_i^*$ is the helmet defined in (13). The radius $\bar{r}_i$ defines the minimum distance from the helmet $\mathcal{H}_i^*$ to the origin. Let x be a point belonging to the intersection of the two ellipsoids $\mathcal{E}(c_i, E_i)$ and $\mathcal{E}(\bar{c}_i, \bar{E}_i)$. Taking δ and μ equal to 1 in Lemma 7, one obtains $x \in \mathcal{C}(0, c_i, \bar{\vartheta}_i, E_i)$ with $\cos(\bar{\vartheta}_i) := \cos(\vartheta_i(1, 1)) = \sqrt{1 - \|E_i c_i\|^{-2}}$ from (24), (19c), and (19a). Now, let us define the set

$$\mathcal{R}_i^* := \mathcal{C}(0, c_i, \bar{\vartheta}_i, E_i) \cap \mathcal{S}_{\geq}(0, \bar{r}_i) \cap \mathcal{E}_{\geq}(c_i, E_i) \cap \mathcal{E}_{\leq}(\bar{c}_i, \bar{E}_i), \tag{28}$$

whose geometry is sketched in Fig. 4. In particular, it is contained in the set of points on the cone $\mathcal{C}(0, c_i, \bar{\vartheta}_i, E_i)$ that have a distance to the origin greater than the distance $\bar{r}_i$ of the helmet $\mathcal{H}_i^*$ to the origin. The idea is that the vehicle should not start avoiding another obstacle while it is still in $\mathcal{R}_i^*$, otherwise there is no guarantee that the number of times the vehicle avoids obstacles is bounded and that global attractivity holds. This leads to the next definition.

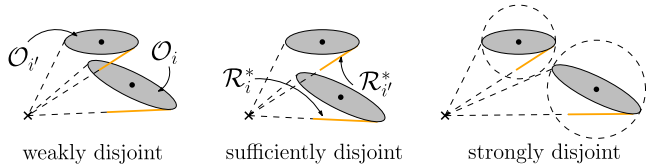

Fig. 4. Different types of disjointness introduced in this article with set $\mathcal{R}_i^*$ (orange) in (28). For global attractivity, sufficient disjointness is asked.

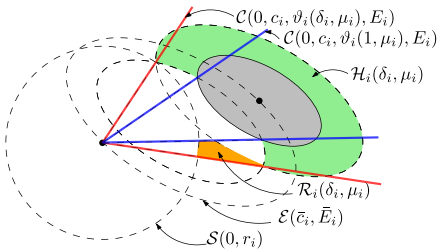

Fig. 5. Safety helmet $\mathcal{H}_i(\delta_i, \mu_i)$ (green) and the corresponding escape region $\mathcal{R}_i(\delta_i, \mu_i)$ (orange). The region $\mathcal{R}_i(\delta_i, \mu_i)$ must not intersect with any other jump set $\mathcal{J}_0^{i'}$, $i' \neq i$, to avoid starting another avoidance while the distance to the target has not decreased yet.

Definition 2: The ellipsoids $\{\mathcal{E}(c_i, E_i)\}_{i\in\mathbb{I}}$ are sufficiently pairwise disjoint if they are weakly pairwise disjoint and for all $i, i' \in \mathbb{I}$ with $i \neq i'$, $\mathcal{R}_i^* \cap \mathcal{E}_{\leq}(c_{i'}, E_{i'}) = \emptyset$.

Now, let us introduce the ingredients for a "dilated" version of $\mathcal{R}_i^*$ as in (31) and refer to Fig. 5. First, consider the *escape annulus cone* where solutions escape from the avoidance mode by applying the stabilization vector field. This region lies between the two cones $\mathcal{C}(0, c_i, \vartheta_i(1, \mu_i), E_i)$ and $\mathcal{C}(0, c_i, \vartheta_i(\delta_i, \mu_i), E_i)$, which are related, according to Lemma 7, to the intersections $\mathcal{E}(c_i, E_i) \cap \mathcal{E}(\bar{c}_i, \mu_i \bar{E}_i)$ and $\mathcal{E}(c_i, \delta_i E_i) \cap \mathcal{E}(\bar{c}_i, \mu_i \bar{E}_i)$, respectively. Second, consider for each obstacle $i \in \mathbb{I}$ the ball $\mathcal{S}_{\geq}(0, r_i)$ where the radius r_i is defined by $r_i^2 := \min\{\|x\|^2 : x \in \mathcal{H}_i(\delta_i, \mu_i)\}$. Note that the safety helmet $\mathcal{H}_i(\delta_i, \mu_i)$ is nonempty and compact; hence, a scalar r_i exists. Moreover $r_i > 0$ for each $i \in \mathbb{I}$ because $\|\delta_i E_i c_i\| = \delta_i \underline{\delta}_i^{-2} > \delta_i \underline{\delta}_i^{-1} > 1$ by Assumption 2 and the selection of δ_i in Table I, so that $0 \notin \mathcal{E}_{\leq}(c_i, \delta_i E_i)$ and in turn $0 \notin \mathcal{H}_i(\delta_i, \mu_i)$ since $\mathcal{H}_i(\delta_i, \mu_i) \subset \mathcal{E}_{\leq}(c_i, \delta_i E_i)$. Finally, we can define a "dilated" version of $\mathcal{R}_i^*$ as

$$\mathcal{R}_i(\delta_i, \mu_i) := \mathcal{S}_{\geq}(0, r_i) \cap \mathcal{E}_{\geq}(c_i, \delta_i E_i) \cap \mathcal{E}_{\leq}(\bar{c}_i, \bar{E}_i) \cap \mathcal{C}_{\geq}(0, c_i, \vartheta_i(1, \mu_i), E_i) \cap \mathcal{C}_{\leq}(0, c_i, \vartheta_i(\delta_i, \mu_i), E_i). \quad (31)$$

Lemma 8: Assume that the obstacles $\{\mathcal{O}_i\}_{i\in\mathbb{I}}$ are sufficiently pairwise disjoint. Then, for each $i \in \mathbb{I}$, there exist δ_i^*, μ_i^* such that for all $\delta_i \in (\delta_i^*, 1)$ and $\mu_i \in (1, \mu_i^*)$, we have

$$\forall i,' i'' \in \mathbb{I}, i' \neq i,'' \ \mathcal{R}_{i'}(\delta_{i'}, \mu_{i'}) \cap \mathcal{E}_{\leq}(c_{i''}, \delta_{i''} E_{i''}) = \emptyset. \quad (32)$$

Property (32) of Lemma 8 is used to show global attractivity. Intuitively, we require that after avoiding an obstacle, the distance $\|x\|$ to the target decreases before the vehicle reaches the proximity of another obstacle. Although the bounds δ_i^* and μ_i^* are not defined explicitly for generic ellipsoids, the parameters δ_i and μ_i can be tuned offline. Next is our main result for this section, proven in the Appendix.

Theorem 2: Consider the hybrid system (22) under the same assumptions as Theorem 1. Assume also that the obstacles $\{\mathcal{O}_i\}_{i\in\mathbb{I}}$ are sufficiently pairwise disjoint, and the δ_i's and μ_i's are tuned so that (32) holds. Then, the set $\mathcal{A} := \{0\} \times \mathbb{I} \times \mathbb{M}$ is globally asymptotically stable for (22) and the number of jumps is bounded.

For spherical obstacles, we show next that the extra tuning of the parameters to satisfy (32) is not needed. The proof is in [21].

Theorem 3: (Spherical obstacles) Let $E_i = \lambda_i I_n$ for all $i \in \mathbb{I}$. Under the same assumptions as Theorem 1, the set $\mathcal{A} := \{0\} \times \mathbb{I} \times \mathbb{M}$ is globally asymptotically stable for (22) and the number of jumps is bounded.

C. Complementary Properties

1) Bounded Control: First, solutions initialized within a certain compact ball always remain there. Indeed, let $\mathcal{S}_{\leq}(0, r_b)$, with $r_b > 0$, be the smallest ball containing all the dilated ellipsoids $\mathcal{E}(c_i, \delta_i E_i)$ (which must exist since these ellipsoids are compact). During stabilization mode the distance $\|x\|$ is decreasing and during avoidance mode the vehicle stays within the dilated ellipsoids $\mathcal{E}(c_i, \delta_i E_i)$. Then, it is guaranteed that from all $x(0, 0) \in \mathcal{S}_{\leq}(0, r_b)$, all solutions satisfy $x(t, j) \in \mathcal{S}_{\leq}(0, r_b)$ for all $(t, j) \in \operatorname{dom} x$. Moreover, since the projection matrix $\pi^{\perp}(E_i(x - c_i))$ has eigenvalues in 0 and 1, it follows that we can upper bound the control input in (10) by $\|u\| \leq k\alpha(r_b + p)$ where $k = \max\{k_1, k_0, k_{-1}\}$, $\alpha = \max_{i\in\mathbb{I}}(\lambda_{\max}(E_i)/\lambda_{\min}(E_i))$ and $p = \max_{i\in\mathbb{I}} \|p_1^i\|$. The control gains can then be tuned to satisfy the inherent practical saturation of the actuators.

2) Semiglobal Preservation: This property [17, Sec. II] is desirable when the original controller parameters are optimally tuned and the controller modifications imposed by the presence of the obstacles should be as minimal as possible. Such a property is also accounted for in the quadratic programming formulation of [28, III.A]. In our case, we have the next proposition, whose proof is given in [21].

Proposition 1: Let $\epsilon \in (0, 1)$ and $\mathcal{W}_\epsilon := \bigcap_{i\in\mathbb{I}} \mathcal{E}_{\geq}(c_i, \epsilon E_i)$. There exist controller parameters such that the control law matches, in $\mathcal{W}_\epsilon$, the stabilization feedback $u = -k_0 x$ ($k_0 > 0$) used in the absence of obstacles.

3) Nonpoint Mass Vehicles: There is no loss of generality in considering a point-mass vehicle in this article. In fact, let us consider a vehicle with some volume, e.g., bounded by $\mathcal{S}_{\leq}(x, r_v)$. Then, in a feasible navigation scenario, the radius r_v of the vehicle needs to be smaller than the smallest distance between the obstacles, i.e., for all $i, i' \in \mathbb{I}$ with $i \neq i', r_v < \mathbf{dist}(\mathcal{E}_{\leq}(c_i, E_i), \mathcal{E}_{\leq}(c_{i'}, E_{i'})) := \inf\{|x - x'| : x \in \mathcal{E}_{\leq}(c_i, E_i), x' \in \mathcal{E}_{\leq}(c_{i'}, E_{i'})\}$. For safety of the whole volume of the vehicle, the selection $\epsilon_i < (1 + \lambda_{\max}(E_i) r_v)^{-1}$ is sufficient (in addition to Table I) to guarantee that the vehicle in stabilization mode starts the avoidance mode away from the obstacle. Indeed, under this condition, it is easy to show that for all $x \in \mathcal{E}_{\geq}(c_i, \epsilon_i E_i)$ (i.e., the vehicle center is outside the dilated ellipsoid $\mathcal{E}(c_i, \epsilon_i E_i)$) and for all $x' \in \mathcal{S}_{\leq}(x, r_v)$, one has $x' \in \mathcal{E}_{\geq}(c_i, E_i)$, which guarantees safety of the whole volume of the vehicle.

4) Robustness: The constructed hybrid controller guarantees some level of robustness to perturbations (e.g., in the form of measurement noise). Hysteresis switching is one of the typical ways to ensure robustness to measurement noise, and hysteresis switching is, indeed, behind the designed hybrid feedback, in particular the hysteresis regions of flow and jump sets in Section IV-B and the logical selections of the jump sets in Section IV-C. More generally, fundamental results in [22, Ch. 7] guarantee structurally that global asymptotic stability of $\mathcal{A}$ in Theorem 2 is also uniform (by [22, Th. 7.12]) and robust (by [22, Th. 7.21]) with respect to perturbations since $\mathcal{A}$ is a compact set and the hybrid basic conditions are satisfied as per Lemma 5.

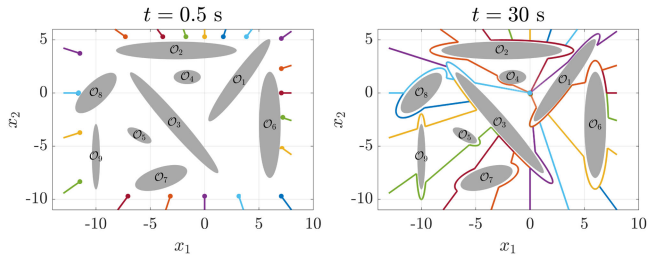

Fig. 6. Plot (at times $t = 0.5$ and $t = 30$ s) of the 2-D trajectory of the vehicle starting at different initial conditions.

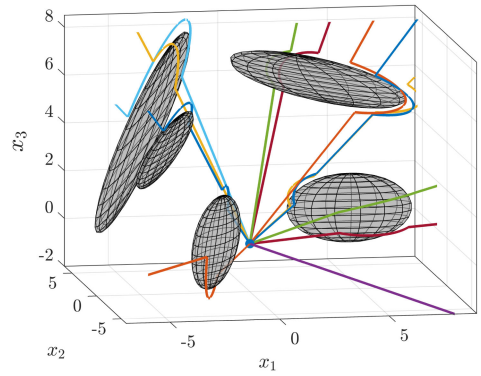

Fig. 7. Plot (at time $t = 30$ s) of the 3-D trajectory of the vehicle starting under different initial conditions.

VI. Simulations

We illustrate the effectiveness of the proposed hybrid control strategy through two simulation scenarios. The first scenario considers nine obstacles in 2-D as in Fig. 6, whereas the second one considers five obstacles in 3-D as in Fig. 7. For both cases, Table I provides a suitable order to choose the parameters for each $i \in \mathbb{I}$, as follows.

1) For $\underline{\delta}_i$ in (19a), select δ_i and ϵ_i so that $\underline{\delta}_i < \delta_i < \epsilon_i < 1$.
2) For δ_i and $\bar{\mu}_i(\delta_i)$ in (19b), select ν_i and μ_i so that $1 < \nu_i < \mu_i < \bar{\mu}_i(\delta_i)$, possibly iterating steps 1 and 2 so that δ_i and μ_i satisfy (32).
3) For δ_i, μ_i and $\bar{\theta}_i(\delta_i, \mu_i)$ in (19c), select ψ_i, $\bar{\psi}_i$ and θ_i so that $0 < \psi_i < \bar{\psi}_i < \theta_i < \bar{\theta}_i(\delta_i, \mu_i)$.

Any parameter selection according to this guideline guarantees our results and can be carried out keeping in mind the physical interpretation illustrated in Section IV-B for these parameters. The gains are $k_0 = k_1 = k_{-1} = 1/4$ and determine the speed of convergence of the scheme. By (11a), the point p_1^i can be selected arbitrarily as long as it is on $\mathcal{C}(c_i, -c_i, \theta_i, E_i)\backslash\{c_i\}$. A suitable choice is given by $p_1^i = \pi^{\perp}(E_i^{-1}\mathbf{R}(\theta_i)E_i c_i)c_i$ where $\mathbf{R}(\theta_i)$ is the standard 2×2 rotation matrix with angle θ_i or the standard 3×3 axis-angle rotation matrix with angle θ_i and an arbitrary vector of $\mathbb{S}^2$ as axis. The idea behind this choice of p_1^i is to project c_i on the plane orthogonal to a rotated version of c_i, in order to obtain the point lying on the cone and closest to the origin. Having all points p_m^i close enough to the origin is an effective way so that k_0, k_1, k_{-1} can take the same values and yield comparable speeds for avoidance and stabilization, independently of the obstacles.

Figs. 6 and 7 show that the solutions generated by the closed-loop hybrid system avoid the 2-D and 3-D obstacles and converge to the origin. The respective complete simulation videos can be found at https://youtu.be/CnXJlhzlzd8 , https://youtu.be/4mzTXPR6D9Y.

Finally, we note that for the very obstacle configuration of the 2-D scenario, the state-of-the-art approach of navigation functions [3], [20] cannot be applied since the condition [20, Th. 3, eq. (23)] is violated for all obstacles except obstacle $\mathcal{O}_5$, where [20, eq. (23)] intuitively corresponds to the fact that obstacles are not too flat and not too close to the target position. [20, eq. (23)] is violated for all obstacles of the 3-D scenario. Moreover, navigation function approaches require tuning a parameter sufficiently large, namely k in [20, eq. (17) and Remark 5] and this may conflict with actuator limitations. Instead, our approach provides a clear tuning guideline for all parameters (given in this section) and actuator limitations can be taken into account (see Section V-C1).

VII. Conclusion

We proposed a novel hybrid feedback on $\mathbb{R}^n$ to solve the obstacle avoidance problem for generic ellipsoidal obstacles, in particular flat and close to the target. Our control strategy ensures global asymptotic stabilization to the target and safety (thus, successful navigation from all initial conditions) while guaranteeing a Zeno-free switching between the avoidance and stabilization modes. Moreover, the control input remains bounded (also in arbitrary proximity to obstacles) and matches semiglobally in the free-state space the nominal feedback used in the absence of obstacles. Future work will be devoted to considering more complex vehicle dynamics (e.g., underactuated and second-order dynamics) and more generic obstacle shapes (e.g., convex obstacles).

Appendix

A. Proof of Theorem 1

Define $\mathbf{S}_{\mathscr{H}}(\mathcal{K})$ as the set of all maximal solutions ϕ to $\mathscr{H} = (\mathcal{F}, \mathbf{F}, \mathcal{J}, \mathbf{J})$ with $\phi(0,0) \in \mathcal{K}$. Each $\phi \in \mathbf{S}_{\mathscr{H}}(\mathcal{K})$ has range $\operatorname{rge}\phi \subset \mathcal{K} = \mathcal{F} \cup \mathcal{J}$ by Lemma 6 and the definition of hybrid solution [22, p. 124], so $\mathcal{K}$ is forward pre-invariant [29, Def. 3.3]. The set $\mathcal{K}$ is in fact forward invariant [29, Def. 3.3] if for each $\xi \in \mathcal{K}$, there exists one solution and each $\phi \in \mathbf{S}_{\mathscr{H}}(\mathcal{K})$ is complete, which we show in the rest of the proof through [22, Prop. 6.10]. In the rest of the proof, let $\mathcal{F}_0^* := \bigcap_{i\in\mathbb{I}} \mathcal{F}_0^i$, $\mathcal{J}_0^* := \bigcup_{i\in\mathbb{I}} \mathcal{J}_0^i$.

Lemma 9: Under the assumptions of Theorem 1, we have for each $i \in \mathbb{I}$ and $m \in \{-1, 1\}$:

1) $\mathcal{J}_0^i = \mathcal{H}_i(\epsilon_i, \nu_i)$,
2) $\mathcal{F}_m^i = \mathcal{H}_i(\delta_i, \mu_i) \cap \mathcal{C}_{\geq}(c_i, c_i - p_m^i, \psi_i, E_i)$,
3) $\partial\mathcal{F}_0^*\backslash\mathcal{J}_0^* \subset \bigcup_{i\in\mathbb{I}} \big(\mathcal{E}(c_i, E_i)\backslash\mathcal{E}_{\geq}(\bar{c}_i, \bar{E}_i)\big)$,
4) $\partial\mathcal{F}_m^i\backslash\mathcal{J}_m^i \subset \mathcal{E}(c_i, E_i)\backslash\big(\mathcal{E}_{\leq}(\bar{c}_i, \mu_i\bar{E}_i) \cup \mathcal{C}_{\leq}(c_i, c_i - p_m^i, \psi_i, E_i)\big)$.

First, let us show that the viability condition

$$\mathbf{F}(x, i, m) \cap \mathbf{T}_{\mathcal{F}}(x, i, m) \neq \emptyset \tag{35}$$

holds for all $(x, i, m) \in \mathcal{F}\backslash\mathcal{J}$. Let $(x, i, m) \in \mathcal{F}\backslash\mathcal{J}$, which implies by (22c) that $(x, i) \in \mathcal{F}_m\backslash\mathcal{J}_m$ for some $m \in \mathbb{M}$, and divide into the cases $m = 0$ and $m \in \{-1, 1\}$. When $m = 0$, from (17), there exists $i \in \mathbb{I}$ such that $x \in \mathcal{F}_0^*\backslash\mathcal{J}_0^*$. If $x \in (\mathcal{F}_0^*)^\circ\backslash\mathcal{J}_0^*$ (hence, x is in the interior of $\mathcal{F}_0^*$), then $\mathbf{T}_{\mathcal{F}_0^*}(x) = \mathbb{R}^n$, so that $\mathbf{T}_{\mathcal{F}}(\xi) = \mathbb{R}^n \times \{0\} \times \{0\}$ and (35) holds. If $x \in \partial\mathcal{F}_0^*\backslash\mathcal{J}_0^*$, which satisfies the set inclusion in Lemma 9, the weak pairwise disjointness of $\{\mathcal{E}(c_i, E_i)\}_{i\in\mathbb{I}}$ yields

$$\begin{aligned} &x \in \mathcal{E}(c_i, E_i),\ i \in \mathbb{I} \\ &\mathbf{T}_{\mathcal{F}}(x, i, 0) = \mathcal{P}_{\geq}(0, E_i^2(x - c_i)) \times \{0\} \times \{0\}. \end{aligned} \tag{36}$$

By (12) and $x \notin \mathcal{E}_{\geq}(\bar{c}_i, \bar{E}_i)$ by the set inclusion for $\partial\mathcal{F}_0^*\backslash\mathcal{J}_0^*$ in Lemma 9, we obtain $-k_0 x^\top E_i^2(x - c_i) = k_0\|E_i\bar{c}_i\|^2\big(1 - \|\bar{E}_i(x - \bar{c}_i)\|^2\big) > 0$ hence $\kappa(x, i, 0) \in \mathcal{P}_{\geq}(0, E_i^2(x - c_i))$ in (36), and (35) holds for $m = 0$. When $m \in \{-1, 1\}$, we have $i \in \mathbb{I}$ and $x \in \partial\mathcal{F}_m^i\backslash\mathcal{J}_m^i$, which satisfies the set inclusion in Lemma 9, and so

$$\mathbf{T}_{\mathcal{F}}(x, i, m) = \mathcal{P}_{\geq}(0, E_i^2(x - c_i)) \times \{0\} \times \{0\}. \tag{38}$$

$\kappa(x,i,m) \in \mathcal{P}_{\geq}(0, E_i^2(x-c_i))$ in (38) because $-k_m(x-p_m^i)^\top E_i \pi^\perp(E_i(x-c_i))E_i(x-c_i) = 0$, so the viability condition (35) holds for $m \in \{-1,1\}$ as well.

Second, we apply [22, Prop. 6.10]. By it and (35), there exists a nontrivial solution to $\mathscr{H}$ from each initial condition in $\mathcal{K}$. Finite escape times can only occur through flow. They can neither occur for x in the set $\mathcal{F}_{-1}^i \cup \mathcal{F}_1^i$ because $\mathcal{F}_{-1}^i$ and $\mathcal{F}_1^i$ are bounded by their definitions in (18), nor for x in the set $\mathcal{F}_0^*$ because they would make $x^\top x$ grow unbounded, and this would contradict that $\frac{d}{dt}(x^\top x) \leq 0$ by the definition of $\kappa(x,i,0)$ and by (22a). So, all maximal solutions do not have finite escape times. By Lemma 6, $\mathbf{J}(\mathcal{J}) \subset \mathcal{K} = \mathcal{F} \cup \mathcal{J}$. Hence, by [22, Prop. 6.10], all maximal solutions are complete.

B. Proof of Theorem 2

We prove global asymptotic stability of $\mathcal{A}$ by [22, Def. 7.1]. For each $i \in \mathbb{I}$, $\|\delta_i E_i c_i\| = \delta_i \underline{\delta}_i^{-2} > \delta_i \underline{\delta}_i^{-1} > 1$ by Assumption 2 and the selection of δ_i in Table I, so $0 \notin \mathcal{E}_{\leq}(c_i, \delta_i E_i)$. As a consequence, there exists $\varepsilon^* > 0$ such that the ball $\mathcal{S}_{\leq}(0,\varepsilon^*)$ does not intersect with any of the dilated obstacles $\mathcal{E}_{\leq}(c_i, \delta_i E_i)$. It can be shown easily that for each $\varepsilon \in [0, \varepsilon^*]$, the set $\mathcal{S} := \mathcal{S}_{\leq}(0,\varepsilon) \times \mathbb{I} \times \mathbb{M}$ is forward invariant because $\mathcal{S}_{\leq}(0,\varepsilon)$ is disjoint from $\mathcal{J}_0^*$ and the component x of solutions evolves, after at most one jump, with the stabilization mode $\dot{x} = -k_0 x$. Thanks to forward invariance of $\mathcal{S}$, stability of $\mathcal{A}$ for (22) is immediate from [22, Def. 7.1]. Let us prove global attractivity of $\mathcal{A}$. Before that, we need the next result.

Lemma 10: There exists $\sigma > 0$ such that for all solutions $\xi = (x,i,m)$ with $\xi(t,j) \in \mathcal{F}_l \times \{l\}$ for some $l \in \{-1,1\}$ and $(t,j) \in \operatorname{dom}\xi$, there exists $(s,\ell) \in \operatorname{dom}\xi$ such that $(s,\ell) \succeq (t,j)$ and $\|x(s,\ell)\| \leq \|x(t,j)\| - \sigma$.

Now, for each solution ξ to (22), there exists a finite time $(T,J) \succeq (0,0)$ after which the solution does not evolve with the avoidance controller any longer, i.e., $m(t,j) = 0$ for all $(t,j) \succeq (T,J)$. Otherwise, there would exist a sequence of hybrid times $\{(t_k,j_k)\}_{k=0}^{\infty}$ such that $\xi(t_k,j_k) \in \mathcal{F}_{l_k} \times \{l_k\}$ with $l_k \in \{-1,1\}$ and this would imply by Lemma 10 that $\|x(t_{k+1},j_{k+1})\| \leq \|x(t_k,j_k)\| - \sigma$ for all $k \in \mathbb{N}$. This is, indeed, a contradiction as it would lead to $\|x(\cdot,\cdot)\|$ becoming negative. Then, the solution ξ enters the stabilizing mode $m = 0$ after (T,J) and its flow map $\dot{x} = -k_0 x$ guarantees in turn global attractivity. Moreover, J is the maximum number of jumps of the hybrid system since any extra jump will cause m to take values in $\{-1,1\}$, which is not possible after (T,J).

REFERENCES

[1] M. Hoy, A. S. Matveev, and A. V. Savkin, "Algorithms for collision-free navigation of mobile robots in complex cluttered environments: A survey," *Robotica*, vol. 33, no. 3, pp. 463–497, 2015.

[2] O. Khatib, "Real-time obstacle avoidance for manipulators and mobile robots," in *Proc. Auton. Robot Veh.*, 1986, pp. 396–404.

[3] D. E. Koditschek and E. Rimon, "Robot navigation functions on manifolds with boundary," *Adv. Appl. Math.*, vol. 11, no. 4, pp. 412–442, 1990.

[4] H. G. Tanner and A. Kumar, "Formation stabilization of multiple agents using decentralized navigation functions," in *Proc. Robot.: Sci. Syst.*, vol. 1, 2005, pp. 49–56.

[5] D. V. Dimarogonas, S. G. Loizou, K. J. Kyriakopoulos, and M. M. Zavlanos, "A feedback stabilization and collision avoidance scheme for multiple independent non-point agents," *Automatica*, vol. 42, no. 2, pp. 229–243, 2006.

[6] G. Roussos and K. J. Kyriakopoulos, "Decentralized and prioritized navigation and collision avoidance for multiple mobile robots," in *Distributed Autonomous Robotic Systems*. Berlin, Germany: Springer, 2013, pp. 189–202.

[7] G. Lionis, X. Papageorgiou, and K. J. Kyriakopoulos, "Locally computable navigation functions for sphere worlds," in *Proc. IEEE Int. Conf. Robot. Automat.*, 2007, pp. 1998–2003.

[8] I. Filippidis and K. J. Kyriakopoulos, "Navigation functions for focally admissible surfaces," in *Proc. Amer. Control Conf.*, 2013, pp. 994–999.

[9] S. G. Loizou, "The navigation transformation," *IEEE Trans. Robot.*, vol. 33, no. 6, pp. 1516–1523, Dec. 2017.

[10] C. Vrohidis, P. Vlantis, C. P. Bechlioulis, and K. J. Kyriakopoulos, "Prescribed time scale robot navigation," *IEEE Robot. Autom. Lett.*, vol. 3, no. 2, pp. 1191–1198, Apr. 2018.

[11] A. D. Ames, X. Xu, J. W. Grizzle, and P. Tabuada, "Control barrier function based quadratic programs for safety critical systems," *IEEE Trans. Autom. Control*, vol. 62, no. 8, pp. 3861–3876, Aug. 2017.

[12] P. Falcone, F. Borrelli, J. Asgari, H. E. Tseng, and D. Hrovat, "A real-time model predictive control approach for autonomous active steering," in *Proc. 1st IFAC Int. Workshop NMPC Fast Syst.*, 2006, Art. no. 7.

[13] M. Defoort, A. Kokosy, T. Floquet, W. Perruquetti, and J. Palos, "Motion planning for cooperative unicycle-type mobile robots with limited sensing ranges: A distributed receding horizon approach," *Robot. Auton. Syst.*, vol. 57, no. 11, pp. 1094–1106, 2009.

[14] R. G. Sanfelice, *Robust Hybrid Control Systems*. PhD thesis, University of California, Santa Barbara, 2007.

[15] R. G. Sanfelice, M. J. Messina, S. E. Tuna, and A. R. Teel, "Robust hybrid controllers for continuous-time systems with applications to obstacle avoidance and regulation to disconnected set of points," in *Proc. Amer. Control Conf.*, 2006, pp. 3352–3357.

[16] J. I. Poveda, M. Benosman, A. R. Teel, and R. G. Sanfelice, "A hybrid adaptive feedback law for robust obstacle avoidance and coordination in multiple vehicle systems," in *Proc. Amer. Control Conf.*, 2018, pp. 616–621.

[17] P. Braun, C. M. Kellett, and L. Zaccarian, "Unsafe point avoidance in linear state feedback," in *Proc. IEEE Conf. Decis. Control*, 2018, pp. 2372–2377.

[18] P. Braun, C. M. Kellett, and L. Zaccarian, "Explicit construction of stabilizing robust avoidance controllers for linear systems with drift," *IEEE Trans. Autom. Control*, vol. 66, no. 2, pp. 595–610, Feb. 2021.

[19] S. Berkane, A. Bisoffi, and D. V. Dimarogonas, "A hybrid controller for obstacle avoidance in an n-dimensional euclidean space," in *Proc. Eur. Control Conf.*, 2019, pp. 764–769.

[20] S. Paternain, D. E. Koditschek, and A. Ribeiro, "Navigation functions for convex potentials in a space with convex obstacles," *IEEE Trans. Autom. Control*, vol. 63, no. 9, pp. 2944–2959, Sep. 2018.

[21] S. Berkane, A. Bisoffi, and D. V. Dimarogonas, "Obstacle avoidance via hybrid feedback," 2021. [Online]. Available: https://arxiv.org/abs/2102.02883

[22] R. Goebel, R. G. Sanfelice, and A. R. Teel, *Hybrid Dynamical Systems: Modeling, Stability, and Robustness*. Princeton, NJ, USA: Princeton Univ. Press, 2012.

[23] C. D. Meyer, *Matrix Analysis and Applied Linear Algebra*. Philadelphia, PA, USA: SIAM, 2000.

[24] C. G. Mayhew and A. R. Teel, "Global stabilization of spherical orientation by synergistic hybrid feedback with application to reduced-attitude tracking for rigid bodies," *Automatica*, vol. 49, no. 7, pp. 1945–1957, 2013.

[25] Y.-K. Choi, W. Wang, Y. Liu, and M.-S. Kim, "Continuous collision detection for two moving elliptic disks," *IEEE Trans. Robot.*, vol. 22, no. 2, pp. 213–224, Apr. 2006.

[26] W. Wang, J. Wang, and M.-S. Kim, "An algebraic condition for the separation of two ellipsoids," *Comput. Aided Geometric Des.*, vol. 18, no. 6, pp. 531–539, 2001.

[27] V. J. Lumelsky and A. Stepanov, "Dynamic path planning for a mobile automaton with limited information on the environment," *IEEE Trans. Autom. Control*, vol. AC-31, no. 11, pp. 1058–1063, Nov. 1986.

[28] L. Wang, A. D. Ames, and M. Egerstedt, "Safety barrier certificates for collisions-free multirobot systems," *IEEE Trans. Robot.*, vol. 33, no. 3, pp. 661–674, Jun. 2017.

[29] J. Chai and R. G. Sanfelice, "Forward invariance of sets for hybrid dynamical systems (Part I)," *IEEE Trans. Autom. Control*, vol. 64, no. 6, pp. 2426–2441, Jun. 2019.